1-1-2014

Colloidal solitary waves with temperature dependent compressibility

Amirah Azmi
University of Wollongong, aa438@uowmail.edu.au

Timothy Marchant
University of Wollongong, tim@uow.edu.au

Colloidal solitary waves with temperature dependent compressibility

Abstract

Spatial solitary waves which form in colloidal suspensions of dielectric nanoparticles are considered. The interactions, or compressibility, of the colloidal particles, is modelled using a series in the particle density, or packing fraction, where the virial, or series, coefficients depend on the type of particle interaction model. Both the theoretical hard disk and sphere repulsive models, and a model with temperature dependent compressibility, are considered. Experimental results show that particle interactions can be temperature dependent and either repulsive or attractive in nature, so we model the second virial coefficient using a physically realistic temperature power law. One- and two-dimensional semi-analytical colloidal solitary wave solutions are found. Trial functions, based on the form of the nonlinear Schrödinger equation soliton, are used, together with averaging, to develop the semi-analytical solutions. When the background packing fraction is low, the one-dimensional solitary waves have three solutions branches (with a bistable regime) while the two-dimensional solitary waves have two solution branches, with a single stable branch. The temperature dependent second virial coefficient results in changes to the solitary wave properties and the parameter space, in which multiple solutions branches occur. An excellent comparison is found between the semi-analytical and numerical solutions.

Keywords

compressibility, colloidal, dependent, temperature, waves, solitary

Disciplines

Engineering | Science and Technology Studies

Publication Details

Azmi, A. & Marchant, T. R. (2014). Colloidal solitary waves with temperature dependent compressibility. Journal of Optics, 16 (5), 1-11.

Colloidal solitary waves with temperature dependent compressibility

A. Azmi[1], **T.R. Marchant**[1]

[1] School of Mathematics and Applied Statistics,
The University of Wollongong,
Wollongong, 2522, N.S.W., Australia.

E-mail: aa438@uow.edu.au, tim_marchant@uow.edu.au

PACS numbers: 42.65.Tg, 42.70.Nq, 02.30.Mv

Abstract. Spatial solitary waves which form in colloidal suspensions of dielectric nanoparticles are considered. The interactions, or compressibility, of the colloidal particles, is modelled using a series in the particle density, or packing fraction, where the virial, or series, coefficients depend on the type of particle interaction model. Both the theoretical hard disk and sphere repulsive models, and a model with temperature dependent compressibility, are considered. Experimental results show that particle interactions can be temperature dependent and either repulsive or attractive in nature, so we model the second virial coefficient using a physically realistic temperature power law. One and two dimensional semi-analytical colloidal solitary wave solutions are found. Trial functions, based on the form of the Nonlinear Schrödinger Equation soliton, are used, together with averaging, to develop the semi-analytical solutions. When the background packing fraction is low, the one dimensional solitary waves have three solutions branches (with a bistable regime) while the two dimensional solitary waves have two solution branches, with a single stable branch. The temperature dependent second virial coefficient results in changes to the solitary wave properties and the parameter space, in which multiple solutions branches occur. An excellent comparison is found between the semi-analytical and numerical solutions.

1. Introduction

In recent years, there has been an increasing interest in the interaction between light and various soft matter media. Many studies in the field discuss the emergence of new tools in optics such as optical tweezers, sensors and traps, which allow selective particle trapping and manipulation, see [1, 2, 3]. The ideas behind these powerful optical manipulation techniques and recent applications in soft matter science are discussed in [4] while [5] summarizes the recent developments in this area. The phenomenon of optical spatial solitary waves has been widely explored, experimentally, theoretically and numerically, for many media, including nematic liquid crystals, [6], photorefractive crystals [7], glasses [8] and thermal media [9]. In all these media solitary waves occur due to a balance between diffraction (in the spatial domain) or dispersion (in the temporal domain) and nonlinear (self-) focusing. In all cases a nonlinear interaction between the medium and the light alters the refractive index of the medium. In the colloidal medium considered here, spatial solitary waves form due to a balance between diffraction of the light beam and the nonlinear particle-light interaction, which attracts the colloidal nanoparticles towards regions of higher light intensity. For spatial solitary waves the solutions have no time dependence but one of the spatial variables is time-like. The equations support both one- and two-dimensional envelope solitary waves which are also termed the (1+1)-D and (2+1)-D cases, due to the propagation variable being time-like in nature.

The compressibility of a colloid is usually defined via the non-ideal gas law where the pressure is given as a function of the density, or packing fraction, in a series form. The nature of the interactions between the colloidal nanoparticles defines the virial coefficients of the perturbation series. The classical theoretical repulsive interaction models are the hard disk model, valid in (1+1)-D, and hard sphere model, valid in (2+1)-D. For these models the virial coefficients can be found using integral theories, for the lower-order coefficients, and numerical simulations for the higher-order ones. Typically a series of nine or ten terms is used but uncertainty in the exact values for the higher-order coefficients leads to uncertainties in the occurrence of phase transitions, from liquid to solid. Many authors have explored the calculation of accurate higher-order virial coefficients for the hard disk and sphere models, see, for example, [10, 11, 12]. For the hard sphere model, the Carnahan-Starling (CS) formula represents an accurate analytical approximation, valid for low to medium densities. For the hard disk model, the Scaled Particle Theory (SPT) provides a useful approximation at low to medium densities.

[13] used the hard-sphere CS formula and derived numerically exact propagation constant versus power curves for the (1+1)-D and (2+1)-D cases. In the (1+1)-D case they found bistable behaviour and examined solitary wave interactions for solitary waves of the same power, from the same and different solution branches. Qualitatively different interactions occurred for solitary wave interactions for waves from the same and different branches. [14] considered a colloidal suspension of two different types of nanoparticles. One type was approximated by the CS formula, where the refractive

index is higher than the background medium and the other with refractive index lower than the background medium. Numerical solitary wave solutions showed that bistability can occur in the (2+1)-D case, which does not occur for the single nanoparticle species case. [15] considered the hard-sphere CS model to obtain semi-analytical solutions via an averaged Lagrangian approach, where trial functions are chosen for the solitary waves. The highly accurate semi-analytical solutions allowed analytical estimates of the regions of parameter space, in which multiple solution branches occurred, to be found.

For real fluids, both pure substances and colloidal mixtures, many experimental results are available for the second virial coefficient, which describes the leading density dependent correction to the ideal gas law. This is regarded as one of the key thermodynamic properties, is closely related to the intermolecular forces between two molecules, and is usually temperature dependent, see [16]. [17] obtained experimental results for semiconductor nanocrystals in Toluene solution. Experimental results show the second virial coefficient is an increasing function of temperature, with the coefficient changing from a negative value to a positive one. This change in sign indicates that the pairwise forces on the molecules change from attractive to repulsive as the temperature increases. [18] considered synthetic polymeric materials with nanoscale particle inclusions, called polyhedral oligomeric sislesquioxanes (POSS). Molecular simulations predict an increase in the second virial coefficient from negative to positive, as temperature increases, for one type of POSS monomers. Another type of POSS monomer initially showed an increase in coefficient, as the temperature increased, but then decreased to larger negative values as the temperature rose further. [19] summarised the behaviour of the second virial coefficient for many types of fluids. They found that the temperature dependence of the coefficient is accurately modeled by a power law form.

In this paper we obtain (1+1)-D and (2+1)-D semi-analytical solitary colloidal wave solutions where the colloidal particle compressibility has a general series form. Section 2 discusses the background of modulation theory and develops the semi-analytical solutions. In section 3, semi-analytical power versus propagation constant and neutral stability curves are obtained for both the (1+1)-D and (2+1)-D cases. Results are presented for the repulsive hard disk and sphere models and for a temperature model where the second virial coefficient can change sign, from repulsive to attractive. These results illustrate the multiplicity of the solitary wave solutions and the regions of parameter space in which they occur. The effect of varying the temperature, on the properties of the solitary waves and on these parameter regions, is also explored in detail. Finally, some concluding remarks and recommendations for future work are made in section 4.

2. Modulation equations

A general form of the equations governing light propagation in colloidal media is used. It is important to note that the colloidal particles have a higher refractive

index than the background liquid medium. So when an optical beam passes through the medium the optical gradient force acts against particle diffusion, increasing the concentration of colloidal particles and hence the refractive index, in regions of higher light intensity, allowing self-focusing to occur. Using these assumptions, we obtain a Nonlinear Schrödinger (NLS) type equation that governs the nonlinear propagation of the beam through a colloidal suspension, see [13],

$$i\frac{\partial u}{\partial z} + \frac{1}{2}\nabla^2 u + (\eta - \eta_0)u = 0, \quad |u|^2 = g(\eta) - g_0, \tag{1}$$
$$g(\eta) = \ln(\eta) + 2B_2\eta + \frac{3}{2}B_3\eta^2 + \cdots, \quad g(\eta_0) = g_0,$$

where u is the electric field envelope, η is the packing fraction of the colloid particles, and η_0 is the background packing fraction. The governing equation is independent of time t but the propagation variable z plays a time like role. Any damping due to Rayleigh scattering can be ignored as the dielectric sphere particle diameter is much smaller than the laser wavelength, see [14, 20]. The relationship $|u|^2 = g(\eta) - g_0$, between the light intensity and the packing fraction, represents an integration of the generalised Fick's law for the optical force on the nanoparticles, see [14, 20]. The particle interactions, or compressibility, is governed by a non-ideal gas law, which is written in series form with general coefficients B_i. The second, B_2, and third, B_3, virial coefficients are written explicitly in (1). The choice of these coefficients allows the effect of different particle interaction models on the properties of the colloidal solitary waves to be considered.

The colloid equations (1) have the Lagrangian formulation

$$L = i(u^* u_z - u_z{}^*) - |\nabla u|^2 + 2(\eta - \eta_0)|u|^2 - 2\eta\ln\eta + 2\eta_0\ln\eta_0 \tag{2}$$
$$+ 2(\eta - \eta_0)(1 + g_0) - 6\eta - 2B_2\eta^2 - B_3\eta^3 + 6\eta_0 + 2B_2\eta_0^2 + B_3\eta_0^3 + \cdots,$$

where the asterisk superscript denotes the complex conjugate. Previously researchers have developed approximate solutions for NLS-type equations using a Lagrangian formulation with a choice of suitable trial functions [21, 22]. This is based on employing a trial function, that represents the solitary wave, in the variational formulation of the governing equations (1). The trial function approximation method has proved to generate very accurate solutions that match the numerical and experimental results closely, see [23, 24]. To obtain accurate solutions for (1) it is important to identify suitable trial functions for u and η to substitute into the Lagrangian. However, some characteristics of the beam, such as its velocity and position, are independent of the form of the trial functions used for the solitary wave profile, see [25, 26]. This approximate technique is closely related to modulation theory of Whitham and other interrelated perturbation techniques [27]. Here we apply the technique to (1) to obtain both (1+1)-D and (2+1)-D solitary waves.

2.1. The (1+1) spatial dimension waves

We will now look at the solitary wave solutions for the (1+1)-D form of the colloid equations (1), which are functions of the two spatial coordinates, x and z, where z plays

the time-like role. We are only concerned here with steady-state envelope solitary waves (where the envelope is only a function of x) so choose trial functions for the electric field and colloid packing fraction in (1+1)-D as

$$u(x,z) = a\ \mathrm{sech}\frac{x}{w}e^{i\sigma z}, \quad \eta(x) = \eta_0 + \alpha\ \mathrm{sech}^2\frac{x}{\beta}. \tag{3}$$

The solitary wave (3) can be chosen as stationary without loss of generality, as a non-zero velocity can be scaled out of the equations. The electric field component of the solitary wave is based on the NLS soliton sech profile. The form for the packing fraction η is chosen as a sech^2 profile as η is a function of the light intensity $|u|^2$ and $\eta \to \eta_0$ far from the light pulse. σ is the propagation constant of the solitary wave while the other parameters are the amplitude and widths of the pulses. A more complete version of the trial functions could be chosen, which describes the evolution of an initial beam, to a steady solitary wave solution, however these details are not necessary for this study.

We now substitute the trial functions (3) into the Lagrangian (2) and the averaged Lagrangian is obtained by integrating in x over the infinite domain, giving

$$\begin{aligned}
\mathcal{L} &= -4a^2w\sigma - \frac{2}{3}\frac{a^2}{w} + 4\alpha a^2\Omega_1(w,\beta) - 4\beta\Theta_1(\alpha) \\
&+ 4\alpha\beta(1+g_0) - 8B_2\alpha\beta\eta_0 - \frac{8}{3}B_2\alpha^2\beta - 6B_3{\eta_0}^2\alpha\beta - 4B_3\eta_0\alpha^2\beta \\
&- \frac{16}{15}B_3\alpha^3\beta, \quad \text{where} \quad \Omega_1(w,\beta) = \int_0^\infty \mathrm{sech}^2\frac{\zeta}{\beta}\mathrm{sech}^2\frac{\zeta}{w}\mathrm{d}\zeta \\
\Theta_1(\alpha) &= \int_0^\infty \left[\eta_0\ln(1+\frac{\alpha}{\eta_0}\mathrm{sech}^2\zeta) + \alpha\mathrm{sech}^2\zeta\ln(\eta_0+\alpha\mathrm{sech}^2\zeta)\right]\mathrm{d}\zeta.
\end{aligned} \tag{4}$$

The modulation equations, found by taking variations of the averaged Lagrangian wrt all the parameters, are

$$\begin{aligned}
&3\alpha w(\Omega_1 - w\Omega_{1w}) - 1 = 0, \quad \sigma = -\frac{1}{2w^2} + \frac{\alpha}{w}(2\Omega_1 - w\Omega_{1w}), \\
&4a^2\alpha(\Omega_1 - \beta\Omega_{1\beta}) - 4\beta(\alpha\Theta_{1\alpha} - \Theta_1) - \frac{8}{3}B_2\alpha^2\beta - 4B_3\eta_0\alpha^2\beta \\
&- \frac{32}{15}B_3\alpha^3\beta = 0, \\
&\alpha a^2\Omega_{1\beta} - 4\Theta_1 + 4\alpha(1+g_0) - 8B_2\alpha\eta_0 - \frac{8}{3}B_2\alpha^2 - 6B_3\eta_0^2\alpha \\
&- 4B_3\eta_0\alpha^2 - \frac{16}{15}B_3\alpha^3 = 0.
\end{aligned} \tag{5}$$

There are three equations for the five unknowns w, β, α, a and η_0 with the propagation constant σ given by an explicit expression. Hence they represent a two-parameter family of solitary waves. By solving these transcendental equations, it is possible to obtain the optical power,

$$P = \int_{-\infty}^{\infty} |u(x)|^2\mathrm{d}x = 2a^2w, \tag{6}$$

for a (1+1)-D semi-analytical colloidal solitary wave.

2.2. The (2+1) spatial dimension waves

We now consider the propagation of a (2+1)-D beam where the modulation equations of the (1+1)-D beam from the previous section is extended. For this case, the trial functions, which are a natural extension of those in (1+1)-D, are

$$u(x,y,z) = a\mathrm{sech}\frac{\phi}{w}e^{i\sigma z}, \quad \eta(x,y) = \eta_0 + \alpha\mathrm{sech}^2\frac{\phi}{\beta}, \quad \phi = \sqrt{x^2+y^2} \tag{7}$$

Here the waves are functions of the three spatial dimensions but again z is time like, hence they are termed (2+1)-D solitary waves. We will obtain the averaged Lagrangian for the (2+1)-D case by integrating the new Lagrangian with respect to x and y from $-\infty$ to ∞ to get

$$\begin{aligned}
&\mathcal{L} = -1.386a^2w\sigma - 0.3977a^2 + 2\alpha a^2\Omega_2(w,\beta) + 1.386\alpha\beta^2(1+g_0) \\
&- 2\beta^2\Theta_2(\alpha) - 4.1589\ \alpha\beta^2 - 2.773\ B_2\eta_0\alpha\beta^2 - 0.5909\ B_2\alpha^2\beta^2 \\
&- 2.080\ B_3{\eta_0}^2\alpha\beta^2 - 0.8863\ B_3\eta_0\alpha^2\beta^2 - 0.1864\ B_3\alpha^3\beta^2, \\
&\Omega_2(w,\beta) = \int_0^\infty \zeta\mathrm{sech}^2\frac{\zeta}{\beta}\mathrm{sech}^2\frac{\zeta}{w}\mathrm{d}\zeta, \\
&\Theta_2(\alpha) = \int_0^\infty \zeta\left[\eta_0\ln(1+\frac{\alpha}{\eta_0}\mathrm{sech}^2\zeta) + \alpha\mathrm{sech}^2\zeta\ln(\eta_0+\alpha\mathrm{sech}^2\zeta)\right]\mathrm{d}\zeta.
\end{aligned} \tag{8}$$

The coefficients of (8) represent integrals, for which explicit exact expressions do not exist, so they are written here to four significant figures. The modulation equations with respect to the variables w, β, α and a for the averaged Lagrangian (8) are

$$\begin{aligned}
&\alpha(2\Omega_2 - w\Omega_{2w}) - 0.3977 = 0, \quad \sigma = -\frac{0.5737}{w^2} + 0.7214\frac{\alpha}{w^2}(4\Omega_2 - w\Omega_{2w}), \\
&2a^2\Omega_2 - 2\beta^2\Theta_{2\alpha} + 1.386\beta^2(1+g_0) - 4.159\beta^2 - 2.773B_2\eta_0\beta^2 \\
&- 1.182B_2\alpha\beta^2 - 2.080B_3{\eta_0}^2\beta^2 - 1.773B_3\eta_0\alpha\beta^2 - 0.5591B_3\alpha^2\beta^2 = 0, \\
&\alpha a^2\Omega_{2\beta} - 2\beta\Theta_2 + 1.386\alpha\beta(1+g_0) - 8.3180\alpha\beta - 5.545B_2\eta_0\alpha\beta \\
&- 1.182B_2\alpha^2\beta - 4.159B_3{\eta_0}^2\alpha\beta - 1.773B_3\eta_0\alpha^2\beta - 0.3727B_3\alpha^3\beta = 0,
\end{aligned} \tag{9}$$

From the transcendental equations (9) in the (2+1)-D case we obtain a semi-analytical description of the two-parameter family of colloid solitary waves. The optical power is given by

$$P = \int_0^\infty r|u(r)|^2\mathrm{d}r = \ln(2)a^2w^2. \tag{10}$$

Solving (5) or (9) gives semi-analytical power versus propagation constant curves. Stable branches are given by the parts of the curve with positive slope, $\frac{dP}{d\sigma} > 0$, see [28]. Hence points of neutral stability have the property $\frac{dP}{d\sigma} = 0$. By adding this condition to the four transcendental equations (9) , we obtain a condition for the neutral stability curve, in the σ versus η_0 plane.

3. Results and discussion

This section presents results for the semi-analytical colloidal solitary waves, as derived in the previous section. Both the (1+1)-D and (2+1)-D cases are considered with

the hard disk and sphere models discussed together with results for a temperature dependent model. The classical hard disk, appropriate in a (1+1)-D geometry, and hard sphere, appropriate in a (2+1)-D geometry, formulations model scenarios for which the interaction between colloidal particles is repulsive. However many real colloids have temperature dependent virial coefficients, which can represent repulsive or attractive interactions.

Semi-analytical approximations for the power versus propagation constant and neutral stability curves are obtained for both cases. From the power versus propagation constant curve, we can identify the existence of multiple solution branches and determine solitary wave stability. From the neutral stability curves, parameter values corresponding to the region of parameter space, in which multiple solution branches occur are found.

For the hard sphere and disk models, the virial coefficients used are obtained theoretically or via computer simulation, see [11]. For the hard sphere model, the CS formula accurately describes the compressibility at low to medium densities, see [29]. For the hard disk model, the SPT represents the simplest model, see [30]. Equation (11) and (12) below describe the compressibility series for the hard sphere and disk models. For both models typically five or six series terms are needed, to obtain equivalent results to the CS and SPT theories, at large packing fractions. Here we use a six term series,

$$Z = 1 + 4\eta + 10\eta^2 + 18\eta^3 + 28\eta^4 + 40\eta^5 + 54\eta^6 + \cdots, \tag{11}$$

$$Z = 1 + 2\eta + 3\eta^2 + 4\eta^3 + 5\eta^4 + 6\eta^5 + 7\eta^6 + \cdots, \tag{12}$$

where the terms in equation (11) are obtained from Table 3 in [11] while the terms in equation (12) are from Table I in [12].

We develop a temperature dependent model by using known experimental results as a guide. [11] use the following general relationship

$$B_2 = b - \frac{a}{T^{\beta+1}}, \tag{13}$$

where the second virial coefficient is given as a power law. [11] summarizes the parameter values in (13) for many different choices of fluid. As the non-dimensional temperature T varies, the second coefficient B_2 can change from positive to negative, which changes the particle interaction forces from repulsive to attractive. To model temperature effects for (1+1)-D colloid solitary waves, we use the hard disk coefficients (12) but with (13) as the second virial coefficient coefficient where $b = 2$, $a = 100$ and $\beta = 0$. So in the limit as the temperature becomes large, the model approaches the repulsive hard disk one, as $B_2 \to 2$. For (2+1)-D colloid solitary waves we use the hard sphere coefficients (11) but with (13) as the second virial coefficient coefficient where $b = 4$, $a = 100$ and $\beta = 0$, so $B_2 \to 4$ as the temperature becomes large. From (1) we see that, for a given packing fraction, that the wave intensity $|u|^2 = g(\eta) - g_0$ increases as B_2 increases. Hence for a given packing fraction, our chosen temperature dependence (13) means that higher temperatures are associated with higher wave intensities.

The temperature effects on colloidal solitary waves are explored by using the semi-analytical solutions of (5) and (9) for the (1+1)-D and (2+1)-D cases respectively. The

choice of B_2 allows us to explore the effects on the solitary waves and their stability as the temperature changes and the interaction forces vary between repulsive and attractive cases. Note that for real fluids all the series coefficients would be temperature dependent but experimental data for higher-order virial coefficients is generally not available.

In (1+1)-D the numerical solutions are obtained by an analytical integration of the steady-state governing equation, which gives an energy conservation law. The energy conservation law is then numerically integrated to obtain exact solitary wave profiles on all solution branches, both stable and unstable, of the power versus propagation constant curves. In (2+1)-D the imaginary time iterative method is used to obtain numerically exact solitary wave profiles, see [31]. The imaginary time method does not allow unstable solution branches to be found.

3.1. (1+1)-D hard sphere model

The hard sphere model is examined using the compressibility series (11) to confirm that the approximate solutions are accurate and also to examine any differences that occur between this series and the CS formulation, as used by [13, 15], in their studies of colloidal solitary waves.

Figure 1 shows the power versus propagation constant, P versus $\log\sigma$, curve for (1+1)-D hard sphere colloidal solitary waves. The background packing fraction $\eta_0 = 1 \times 10^{-3}$. The same parameters as in figure 1 of [15] are used. Shown are the semi-analytical solutions (5) for the hard sphere series and the CS model and the numerical solutions of (1) for the hard sphere series. The figure shows the existence of two stable branches, separated by an unstable branch. On the low power branch broad solitary waves of small amplitude occur, while on the high power branch the solitary waves are narrower with higher amplitudes. The semi-analytical hard sphere series unstable branch exists for

$$\begin{aligned} &-2.73 < \log\sigma < -1.25 \quad \text{and} \quad 33.26 < P < 51.27, \\ &4.28 \times 10^{-3} < \alpha < 0.19 \quad \text{and} \quad 1.31 < a < 2.28, \\ &3.31 < \beta < 6.62 \quad \text{and} \quad 4.93 < w < 9.69. \end{aligned} \tag{14}$$

The limits of the unstable branch, and the properties of these marginally stable solitary waves are very close to the equivalents for CS solitary waves, with variations less than 1%, see (36) in [15]. These limits and the figure indicate that the series (11) generates solitary wave solutions very similar to those found by the CS formula with both curves the same to graphical accuracy. An excellent comparison with numerical solutions is also found.

Figure 2 shows the power versus propagation constant, P versus $\log\sigma$, curve for (1+1)-D hard sphere colloidal solitary waves. The background packing fraction $\eta_0 = 1 \times 10^{-2}$. Shown are the semi-analytical solutions (5) for the hard sphere series and the CS model and the numerical solutions of (1) for the hard sphere series. Here the bistability has vanished and only a single stable solutions branch exists. The larger

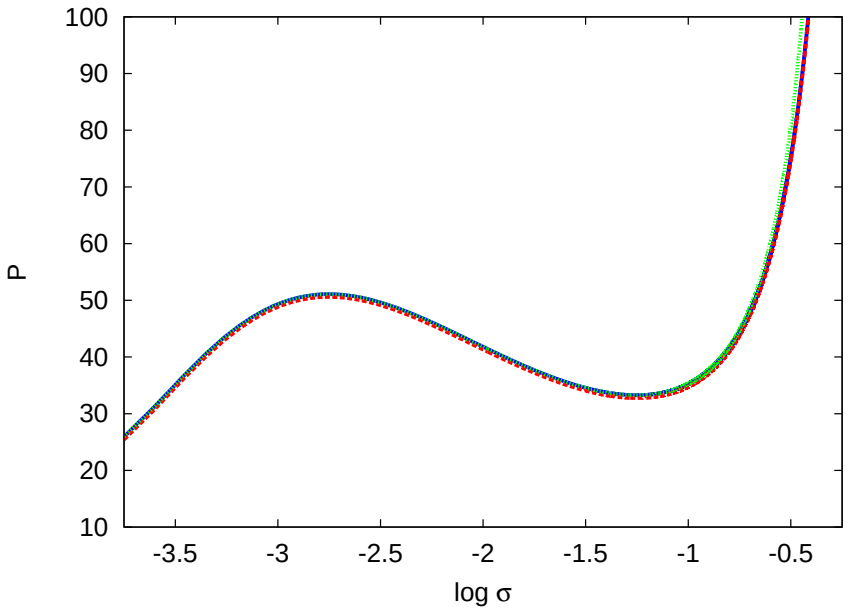

Figure 1. (color online) The power versus propagation constant, P versus $\log\sigma$, curve for (1+1)-D hard sphere models. Shown are the semi-analytical solutions for the hard sphere series (11) (solid blue line) and CS model (dotted green line) and the numerical hard sphere series (dashed red line) solutions. The background fraction is $\eta_0 = 1 \times 10^{-3}$.

value of background packing fraction has resulted in the loss of the multiple solution branches. Again the hard sphere series, the CS formulations and numerical solutions are all very close. The results show that the hard sphere series differ from the CS results, by less than 4%, over the presented range. This is due to the fact differences between the series (11) and the CS formula, occur for high amplitude solitary waves, which have high packing fractions.

Figure 3 shows the neutral stability curve in the propagation constant versus background packing fraction, $\log\sigma$ versus η_0, plane for the (1+1)-D hard sphere colloidal solitary waves. Shown are the semi-analytical solutions (5) for the hard sphere series and the CS model and the numerical solutions of (1) for the hard sphere series. The region under the curves represents parameter values corresponding to the existence of the middle, unstable branch of solitary wave solutions. The region of parameter space in which unstable solutions occur is reduced and then eliminated as the background packing fraction increases. The parameters of the solitary wave with neutral stability at the turning point are $(\log\sigma, \eta_0) = (-1.66, 5.66\times10^{-3})$ for the semi-analytical hard sphere series solution and $(\log\sigma, \eta_0) = (-1.66, 5.61 \times 10^{-3})$ for the numerical solution. This limiting parameter value is also very close to that found by [15] for CS solitary waves, $(\log\sigma, \eta_0) = (-1.67, 5.69 \times 10^{-3})$. So bistable behavior only occurs when background packing fraction, $\eta_0 \leq 5.66 \times 10^{-3}$ and a single stable branch exists for background packing fractions greater than this value. The two semi-analytical predictions and the numerical solutions are all very close to each other with less than a 1% difference.

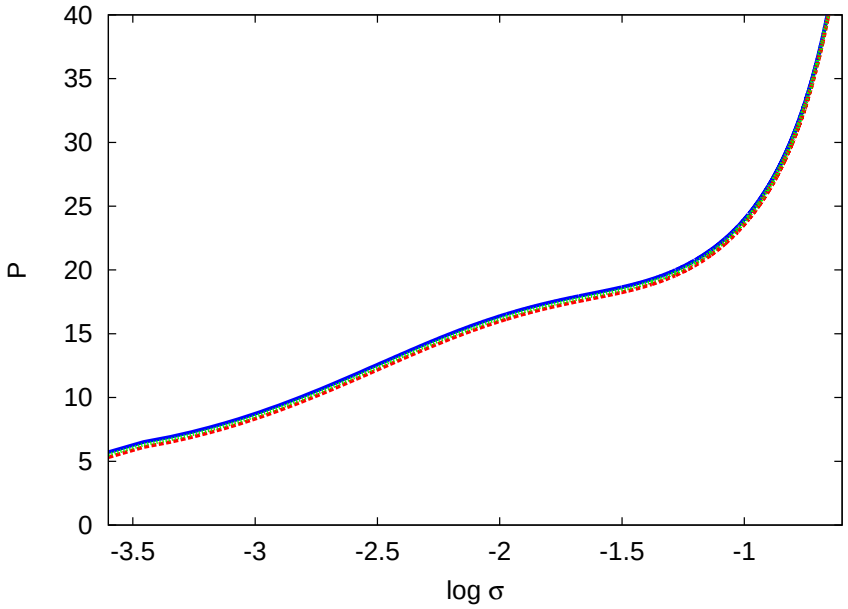

Figure 2. (color online) The power versus propagation constant, P versus $\log\sigma$, curve for (1+1)-D hard sphere models. Shown are the semi-analytical solutions for the hard sphere series (11) (solid blue line) and CS model (dotted green line) and the numerical hard sphere series (dashed red line) solutions. The background fraction is $\eta_0 = 1 \times 10^{-2}$.

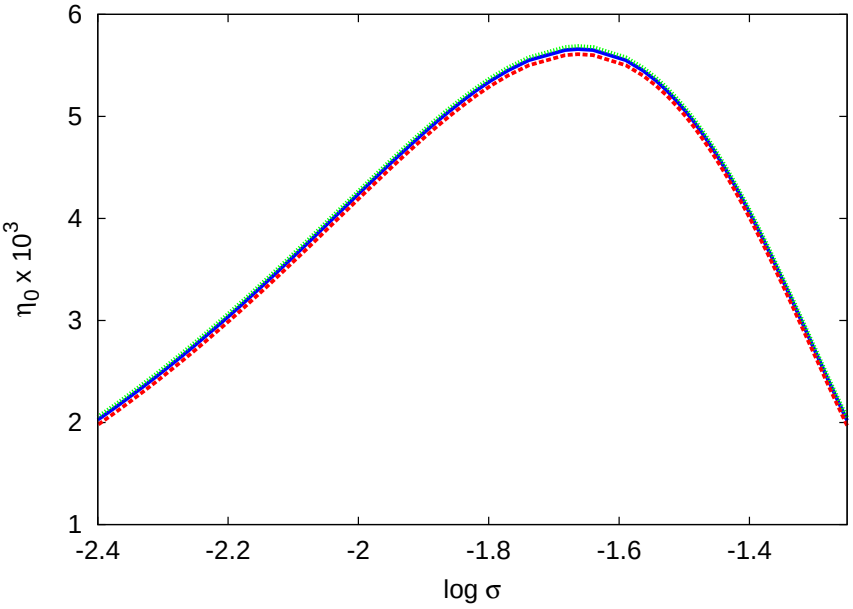

Figure 3. (color online) The neutral stability curve in the propagation constant-background packing fraction, $\log\sigma$ versus η_0, plane for the (1+1)-D hard sphere models. Shown are the semi-analytical solutions for the hard sphere series (11) (solid blue line) and the CS formula (dotted green line), and the numerical hard sphere series (dashed red line) solutions.

3.2. (1+1)-D hard disk model

Many previous studies use the CS compressibility formula even though it is based on the interactions between spherical particles and is not appropriate for modelling (1+1)-D colloidal solitary waves, as they only involve the x and z spatial coordinates. In (1+1)-D scenarios the interaction model should be based on a 2-D geometry, which is consistent with the hard disk model. Here we find (1+1)-D hard disk colloidal solitary waves and compare the results with those for the hard sphere model.

Figure 4 shows the power versus propagation constant, P versus $\log\sigma$, curve for (1+1)-D hard disk solitary waves. The background packing fraction $\eta_0 = 1 \times 10^{-3}$. Shown are the the semi-analytical solutions (5) and numerical solutions of (1). Qualitatively the curve is similar to figure 1, for the hard sphere model, with bistability occurring, but some quantitative differences occur between the two models. For the hard disk model the middle unstable branch exists for

$$\begin{aligned} &-2.76 < \log\sigma < -0.93 \quad \text{and} \quad 23.8 < P < 50.3, \\ &4.47 \times 10^{-3} < \alpha < 0.42 \quad \text{and} \quad 1.31 < a < 2.78, \\ &0.80 < \beta < 10.9 \quad \text{and} \quad 1.54 < w < 14.6. \end{aligned} \tag{15}$$

The end points of the unstable branch, for the hard disk and sphere models, are very similar to each other. If we compare the hard sphere and disk solitary waves for $P = 50$ on the high power branch there are differences in parameter values of about 10% with the hard disk solitary wave a little steeper and narrower than the hard sphere one.

Figure 5 shows the power versus propagation constant, P versus $\log\sigma$, curve for (1+1)-D hard disk model for colloidal solitary waves. The background packing fraction, $\eta_0 = 1 \times 10^{-1}$. Shown are the the semi-analytical solutions (5) and numerical solutions of (1). Again this behaviour is qualitatively similar to the hard sphere case but there are quantitative differences when $\log\sigma > -2$. If we compare the hard sphere and disk solitary waves for $P = 10$ there are significant differences in the wave properties with the hard disk wave much steeper, by about 30%, and narrower, by about 40%, than the CS wave.

Figure 6 shows the neutral stability curve in the propagation constant versus background packing fraction, $\log\sigma$ versus η_0, plane for (1+1)-D hard disk colloidal solitary waves. Both semi-analytical and numerical solutions are shown. The parameters of the solitary waves at the turning point are $(\log\sigma, \eta_0) = (-1.35, 1.14 \times 10^{-2})$ for the semi-analytical solution, and $(\log\sigma, \eta_0) = (-1.35, 1.11 \times 10^{-2})$ for the numerical solution. Hence the semi-analytical model predicts that bistable behaviour occurs for a much greater region of parameter space, compared with the hard sphere model, for which $\eta_0 \leq 5.6 \times 10^{-3}$. Given the significant differences in these predictions of the hard disk and sphere models, and that the hard sphere model is not geometrically appropriate in this scenario, we believe that the hard disk model should be used instead of the hard disk model (or the related CS formula), when modelling (1+1)-D colloidal solitary waves.

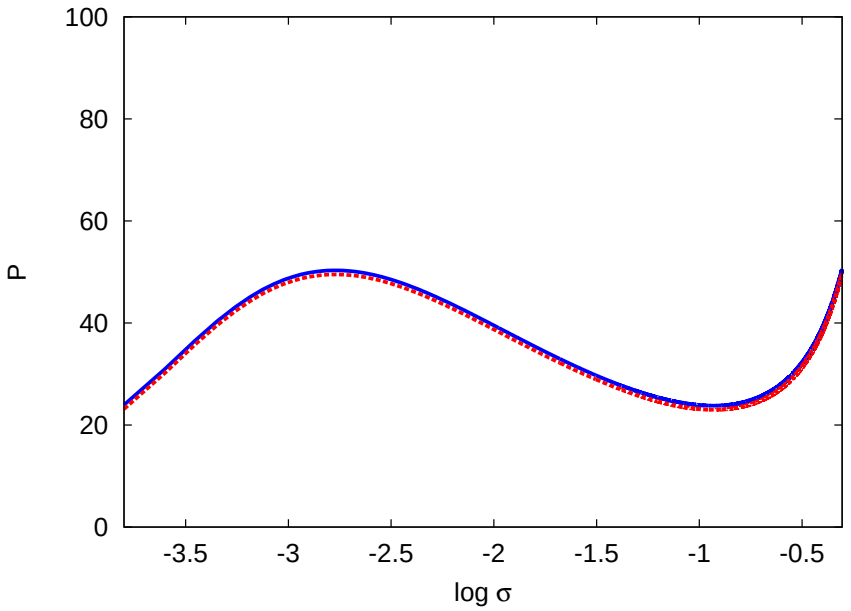

Figure 4. (color online) The power versus propagation constant, P versus $\log\sigma$, curve for the (1+1)-D hard disk model. Shown are the semi-analytical (solid blue line) and the numerical (dashed red line) solutions. The background fraction is $\eta_0 = 1 \times 10^{-3}$

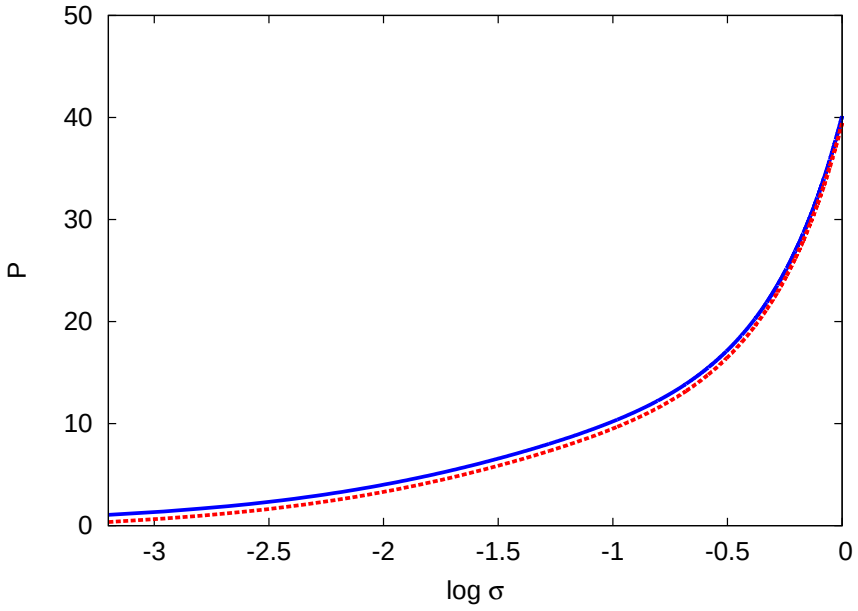

Figure 5. (color online) The power versus propagation constant, P versus $\log\sigma$, curve for the (1+1)-D hard disk model. Shown are the semi-analytical (solid blue line) and the numerical (dashed red line) solutions. The background fraction is $\eta_0 = 1 \times 10^{-1}$

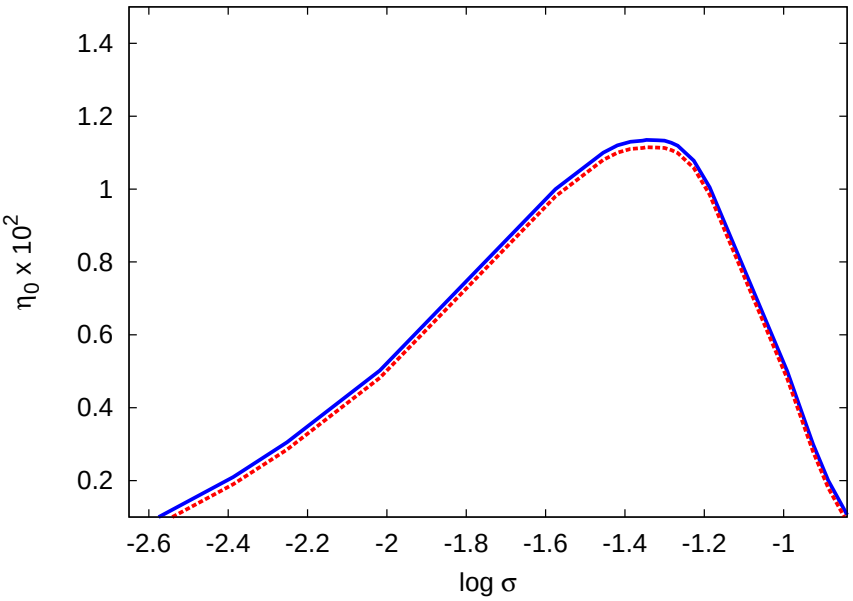

Figure 6. (color online) The neutral stability curve in the propagation constant-background packing fraction, $\log\sigma$ versus η_0, plane for the (1+1)-D hard disk model. Shown are the semi-analytical (solid blue line) and the numerical (dashed red line) solutions.

3.3. (1+1)-D temperature dependent model

We now consider the (1+1)-D hard disk coefficients but with a temperature dependent second coefficient given by (13) and $b = 2$, $a = 100$ and $\beta = 0$. The choice of $\beta = 0$ means that the second coefficient has an inverse temperature dependence. In the limit as the temperature becomes large this model approaches the hard disk case, as $\beta_2 \to 2$.

Figure 7 shows the power versus propagation constant, P versus $\log\sigma$, curves for the (1+1)-D temperature dependent model. The background packing fraction $\eta_0 = 1.0 \times 10^{-3}$ and the temperature is $T = 10, 50$ and 100. Multiple solution branches occur for both $T = 50$ and 100, while for $T = 10$, a single stable branch occurs. The second virial coefficient $B_2 = 0$ at $T = 50$ so for temperatures larger than this the particle interactions are repulsive and for lower temperatures the interactions are attractive. Hence, as the nature of the particle interactions change from repulsive to attractive the bistable nature of the solution disappears. For colloidal solitary waves of the same power, $P = 60$, the solitary waves are much steeper and narrower as the temperature increases and the particle interactions become more repulsive.

Figure 8 shows the neutral stability curve in the propagation constant versus background packing fraction, $\log\sigma$ versus η_0, plane for the (1+1)-D temperature dependent model. Both the semi-analytical and numerical solutions are shown. At $T = 100$, bistable behavior occurs for the (1+1)-D geometry when $\eta_0 \leq 1.47 \times 10^{-3}$, and single stable solution branch exists for background packing fractions greater than this value. For $T = 10$ and $T = 50$ the bistable behavior is possible for $\eta_0 \leq 7.12 \times 10^{-4}$

and $\eta_0 \leq 1.04 \times 10^{-3}$, respectively. As the temperature goes up, the region of parameter space, in which bistability occurs, also increases.

Figure 9 shows the maximum background packing fraction, for which bistability occurs, versus temperature. Shown are semi-analytical and numerical solutions for the (1+1)-D temperature dependent model. As the temperature increases, the maximum background packing fraction, for which bistability is possible, increases. At $T = 1000$ the maximum packing fraction is $\eta_0 = 1.12 \times 10^{-3}$, which is very close to the hard disk limit of $\eta_0 = 1.14 \times 10^{-3}$. The differences between the semi-analytical and numerical solutions are less than 5%.

3.4. (2+1)-D hard sphere model

Here the hard sphere compressibility formula (11) to used to confirm that the (2+1)-D semi-analytical hard sphere colloidal solitary wave solutions are accurate and we also examine any differences that occur with the CS formulation.

Figure 10 shows the power versus propagation constant, P versus $\log \sigma$, curves for (2+1)-D hard sphere colloidal solitary waves. The background packing fraction $\eta_0 = 1 \times 10^{-3}$. Shown are the semi-analytical solutions (9) for the hard sphere series and the CS model and the numerical solutions of (1) for the hard sphere series. This figure indicates the existence of two solution branches, one stable and one unstable. This is qualitatively different to the (1+1)-D case where bistable behavior occurs. The

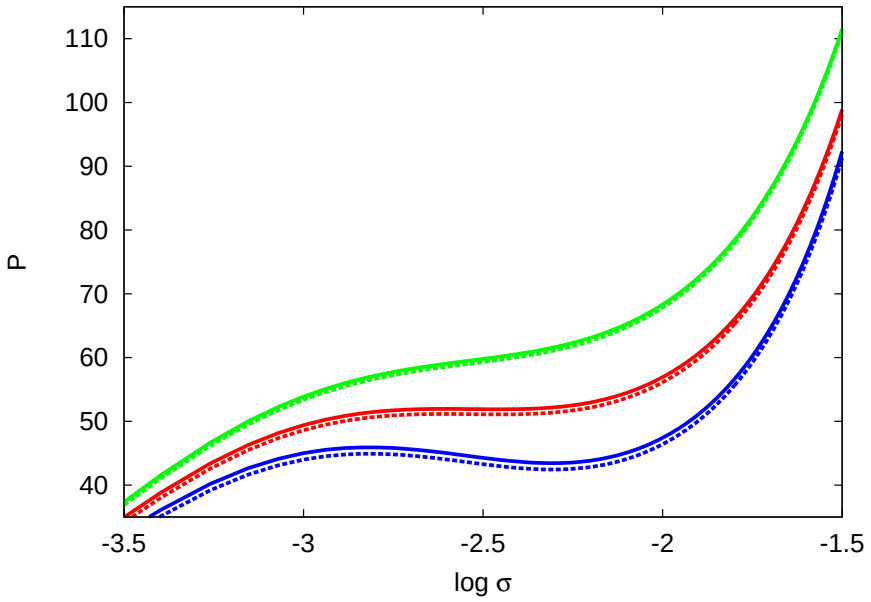

Figure 7. (color online) The power versus propagation constant, P versus $\log \sigma$, curve for the (1+1)-D temperature dependent model. The background fraction is $\eta_0 = 1 \times 10^{-3}$. Shown are the semi-analytical (solid lines) and numerical (dashed lines) results for $T = 10$ (top green lines), $T = 50$ (middle red lines) and $T = 100$ (bottom blue lines).

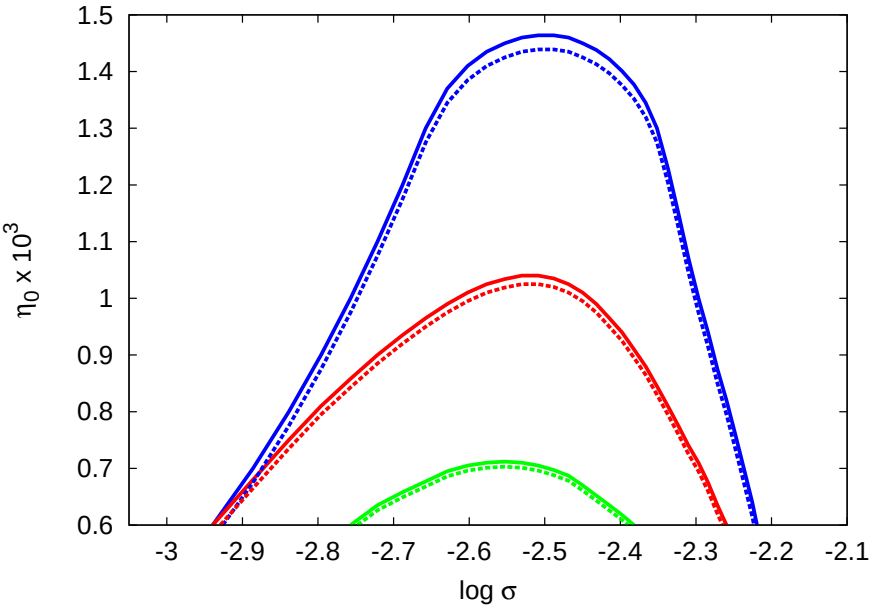

Figure 8. (color online) The neutral stability curve in the propagation constant-background packing fraction plane $(\log\sigma, \eta_0)$ for the (1+1)-D temperature dependent model. Shown are the semi-analytical (solid lines) and numerical (dashed lines) for $T = 10$ (bottom green lines), $T = 50$ (middle red lines) and $T = 100$ (top blue lines).

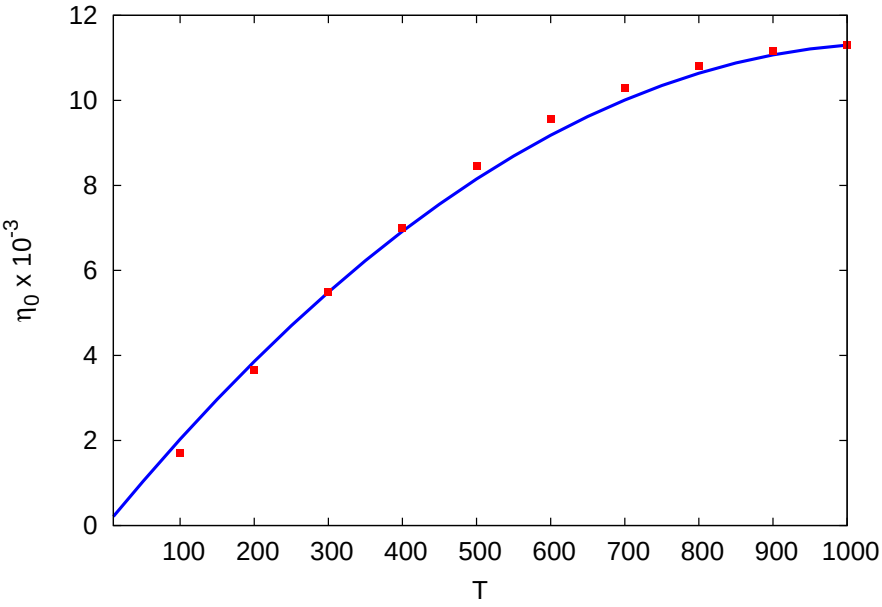

Figure 9. (color online) The maximum background packing fraction, for which bistability occurs, versus temperature. Shown are the semi-analytical (solid blue line) solutions and numerical solutions (red squares) for the (1+1)-D temperature dependent model

(2+1)-D colloidal solitary waves are unstable at small σ (large negative values of $\log\sigma$) because no stable small σ, low power, solutions exists. This is related to the fact that (2+1)-D NLS solitons are unstable, see, for example, [32]. When the power decreases

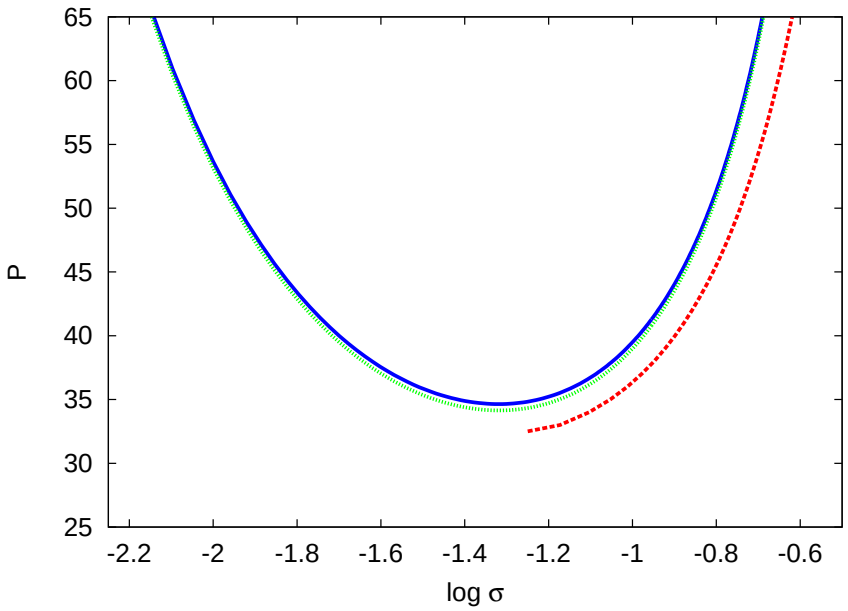

Figure 10. (color online) The power versus propagation constant, P versus $\log\sigma$, curve for (2+1)-D hard sphere models. Shown are the semi-analytical solutions for the hard sphere series (11) (solid blue line) and CS model (dotted green line) and the numerical hard sphere series (dashed red line) solutions. The background fraction is $\eta_0 = 1 \times 10^{-3}$.

the intensity $|u|$ and packing fraction η of the colloidal solitary waves decrease and the governing equation (1) approaches the Kerr limit, resulting in instability for low power (2+1)-D colloidal solitary waves. (1+1)-D colloidal solitary waves also become Kerr-like for small σ and low powers but (1+1)-D NLS solitons are stable, hence the occurrence of a low amplitude stable branch for (1+1)-D colloidal solitary waves.

Comparing the semi-analytical and numerical solutions for the hard sphere series at $\log\sigma = -1.25$ (the smallest $\log\sigma$ for which the numerical solution is stable) there is a 7% difference in the power. The semi-analytical solution predicts that the stable branch occurs for

$$\log\sigma > -1.21, \quad \alpha > 0.48, \quad a > 3.83. \tag{16}$$

Comparing the semi-analytical hard sphere series and CS solutions, we find less than a 1% difference over the range of the figure.

Figure 11 shows the power versus propagation constant, P versus $\log\sigma$, curve for (2+1)-D hard sphere colloidal solitary waves. The background packing fraction $\eta_0 = 1.5 \times 10^{-1}$. Shown are the semi-analytical solutions (9) for the hard sphere series and the CS model and the numerical solutions of (1) for the hard sphere series. In this case there is a single stable solution branch and the comparison between the semi-analytical and numerical solutions is good, with no more than a 10% error. There is also an excellent comparison between the hard sphere series and CS semi-analytical solutions, with the solutions the same to graphical accuracy.

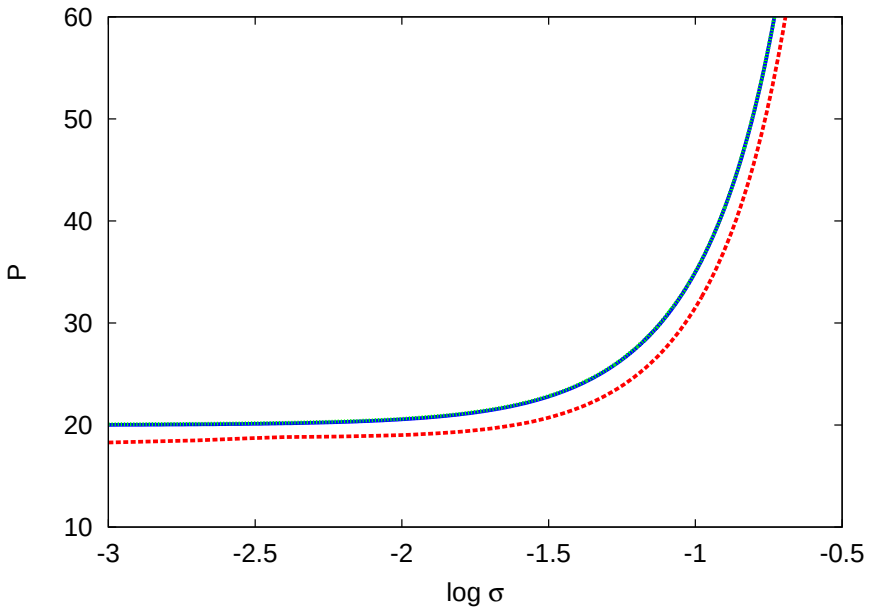

Figure 11. (color online) The power versus propagation constant, P versus $\log\sigma$, curve for (2+1)-D hard sphere models. Shown are the semi-analytical solutions for the hard sphere series (11) (solid blue line) and CS model (dotted green line) and the numerical hard sphere series (dashed red line) solutions. The background fraction is $\eta_0 = 1.5 \times 10^{-1}$.

Figure 12 shows the neutral stability curve in the propagation constant versus background packing fraction, $\log\sigma$ versus η_0, plane for the (2+1)-D hard sphere colloidal solitary waves. Shown are the semi-analytical solutions (9) for the hard sphere series and the CS model and the numerical solutions of (1) for the hard sphere series. Multiple solitary wave solution branches occur for parameter values below the curves. The maximum background packing fraction, for which multiple semi-analytical hrad-sphere series solution branches occur, is $\eta_0 \leq 0.124$. This is extremely close to the numerical estimate of $\eta_0 \leq 0.126$. For the CS case multiple solution branches occur for $\eta_0 \leq 0.125$, so the CS and hard sphere series (11) predictions are very close in this case with a 1% error.

3.5. (2+1)-D temperature dependent model

Here we consider the hard sphere virial coefficients but with a temperature dependent second coefficient given by (13) and $b = 4$, $a = 100$ and $\beta = 0$. As the temperature becomes large the second virial coefficient $B_2 \to 4$ and the hard sphere model is approached.

Figure 13 shows the power versus propagation constant, P versus $\log\sigma$, curve. The background packing fraction $\eta_0 = 1.3 \times 10^{-1}$. Shown are the semi-analytical and numerical results for $T = 10$, 50 and 100. The two curves corresponding to lower temperatures have multiple solution branches while the curve for the highest temperature has a single stable solution branch. The second virial coefficient $B_2 = 0$

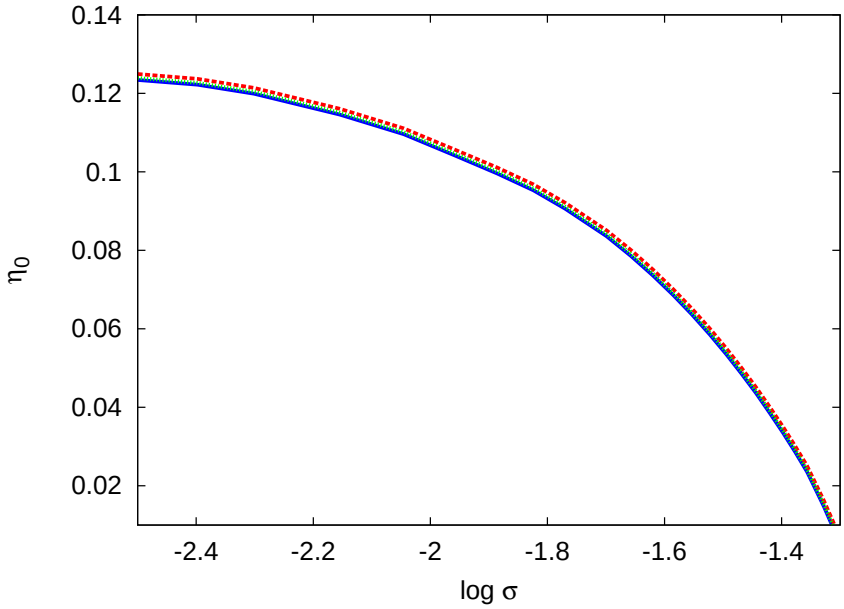

Figure 12. (color online) The neutral stability curve in the propagation constant-background packing fraction, $\log \sigma$ versus η_0, plane for the (1+1)-D hard sphere models. Shown are the semi-analytical solutions for the hard sphere series (11) (solid blue line) and the CS formula (dotted green line), and the numerical hard sphere series (dashed red line) solutions.

at $T = 25$ so solution multiplicity occurs in a larger region of parameter space, as the temperature decreases and the particle interactions become less repulsive, or attractive, in nature. The $T = 50$ curve is very close to the transition between a single solution branch and multiple solution branches. The results from figure 14 show that, for $T = 50$, multiple solution branches occur for $\eta_0 \leq 1.35 \times 10^{-1}$. The comparison between the numerical and semi-analytical solutions is excellent with less than a 5% error. For colloidal solitary waves of the same power, $P = 20$, the solitary waves are much steeper and narrower as the temperature decreases and as the particle interactions become more attractive.

Figure 14 shows neutral stability curves in the propagation constant versus background packing fraction, $\log \sigma$ versus η_0, plane for the (2+1)-D temperature dependent model. Shown are the semi-analytical and numerical results for $T = 25$, 50 and 100. At $T = 25$ multiple solution branches occurs for background packing fraction $\eta_0 \leq 1.44 \times 10^{-1}$, while at higher temperatures $T = 50$ and $T = 100$, the limits for multiple solutions are $\eta_0 \leq 1.35 \times 10^{-1}$, and $\eta_0 \leq 1.27 \times 10^{-1}$, respectively. As the temperature increases, and the repulsion between the particles increases, the parameter region in which multiple solution branches occur, decreases. The comparison between the numerical and semi-analytical solutions is excellent with less than a 1% error.

Figure 15 shows the maximum background packing fraction, for which multiple solutions occur, versus temperature. Shown are the semi-analytical and numerical solutions for the (2+1)-D temperature dependent model. We see that as the temperature

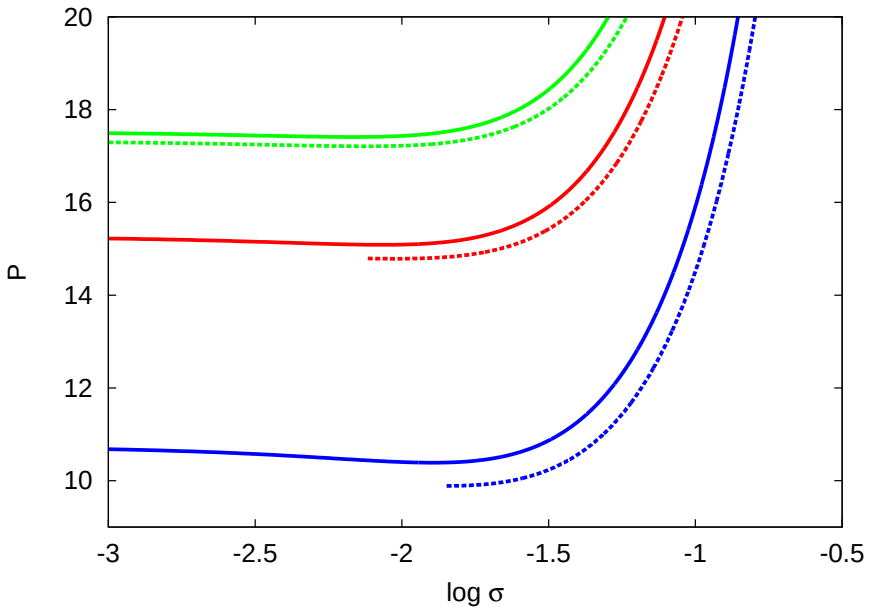

Figure 13. (color online) The power versus propagation constant, P versus $\log \sigma$, curve for the (2+1)-D temperature dependent model. The background fraction is $\eta_0 = 1.3 \times 10^{-1}$. Shown are the semi-analytical (solid lines) and numerical (dashed lines) results for $T = 10$ (bottom blue lines), $T = 50$ (middle red lines) and $T = 100$ (top green lines).

increases, the maximum background packing fraction, for which multiple solution branches occur, decreases. At $T = 350$ the maximum packing fraction is $\eta_0 = 1.26 \times 10^{-1}$, which is close to the hard sphere limit. The differences between the semi-analytical and numerical solutions are less than 4%.

The stability of (2+1)-D colloidal solitary waves is temperature dependent, with the region of parameter space, in which multiple solution branches occurs, decreasing as the temperature increases. For the (1+1)-D temperature dependent model the opposite effect occurs, with as the region of parameter space increasing as the temperature increases (see figure 9). The effect of varying the coefficients in the temperature dependent second virial coefficient (13) have been explored; for all positive choices of a and b the qualitative trends, seen in figure 9, for (1+1)-D colloidal solitary waves, and in figure 15, for (2+1)-D colloidal solitary waves, are the same. Hence the differences in the behaviour of the two cases is due to geometrical effects. There are important differences in the properties of (1+1)-D (stable) and (2+1)-D (unstable) solitons of the related NLS equation, hence it is not surprising that geometrical effects also lead to significant differences in the stability properties of temperature dependent colloidal solitary waves.

4. Conclusions

This paper thoroughly examines semi-analytical solutions for colloidal solitary waves in the (1+1)-D and (2+1)-D geometries. These solutions are described using a series

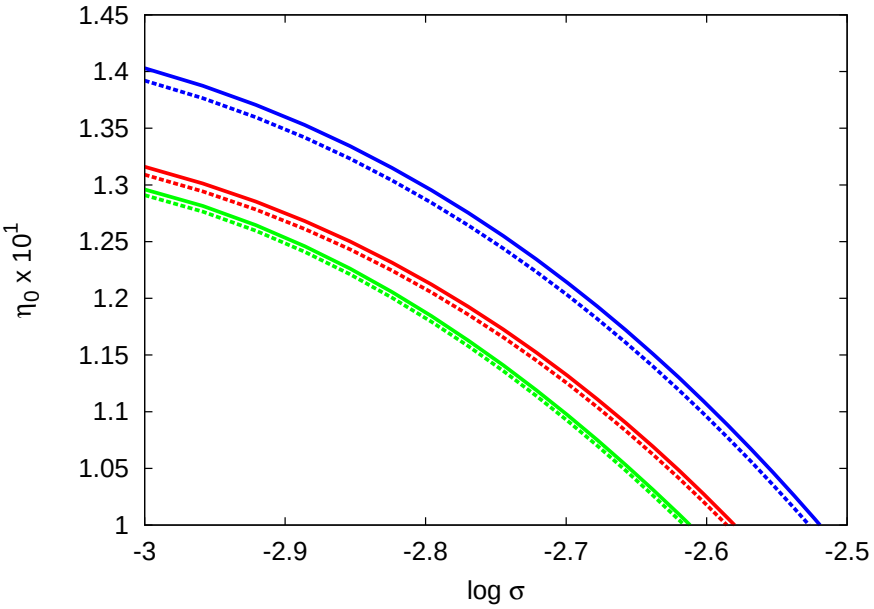

Figure 14. (color online) The neutral stability curve in the propagation constant-background packing fraction plane, $(\log\sigma, \eta_0)$ for the (2+1)-D temperature dependent model. Shown are the semi-analytical (solid lines) and numerical (dashed lines) for $T = 25$ (top blue lines), $T = 50$ (middle red lines) and $T = 100$ (bottom green lines).

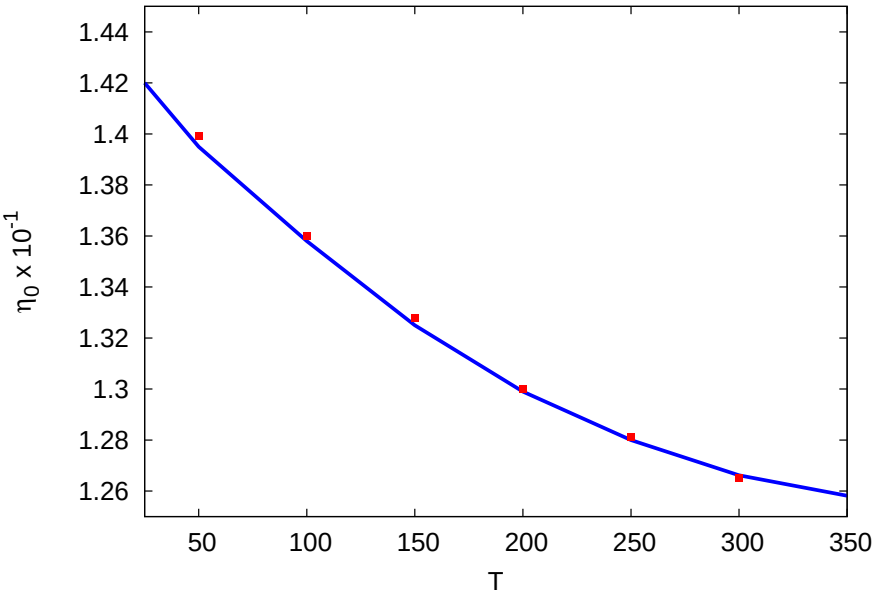

Figure 15. (color online) The maximum background packing fraction, for which multiple solution branches occur, versus temperature. Shown are the semi-analytical (solid blue line) and numerical (red square-point) solutions for the (2+1)-D temperature dependent model

for the non-ideal gas law with hard sphere, hard disk and temperature dependent models all considered. Its shown that, for low to medium packing fractions, the hard sphere formulation is close to the CS approximations, with some differences occurring at large packing fractions. The hard sphere model and its related CS approximation are commonly used to model (1+1)-D colloidal waves, however the interactions between spherical particles is not physically appropriate in this two-dimensional geometry. The (1+1)-D results shown that significant differences occur between the hard disk and hard sphere predictions which indicates that the hard disk model, or some other interaction model consistent with a two-dimensional geometry should be used instead.

The temperature dependent models allow the effects of temperature dependency, on the particle interactions, to be explored. The results show that the regions of parameter space in which multiple solution branches occur vary significantly with temperature. For the (1+1)-D geometry increasing the temperature increases the parameter region in which multiple solutions occur, while for the (2+1)-D geometry the opposite effect occurs, with the parameter region shrinking as the temperature increases. This indicates the importance of geometrical effects on colloidal solitary wave properties and the need to use an appropriate particle interaction model.

An interesting extension to the model considered here would be to include thermal effects, due to the light beam heating the colloid and temperature losses from a finite boundary domain. This model would have some similarities to spatial solitary waves in thermal media [9], but the refractive index would depend both on particle density and temperature.

In summary the formulation of the colloidal equations used here, which incorporates a series form for the compressibility, proves an convenient test bed for exploring different particle interaction models. It is hoped that this theoretical study will encourage experimental investigations of colloidal solitary waves and temperature dependent particle interaction effects.

Acknowledgement: The authors wish to thank two anonymous referees for their comments.

References

[1] Ashkin A 2000 History of optical trapping and manipulation of small-neutral particle, atoms, and molecules *IEEE J. Sel. Top. Quant.* **6** 841–856

[2] Lowen H 2001 Colloidal soft matter under external control *J. Phys. Condens. Mat.*, **13** 415–432

[3] Grier D G 2003 A revolution in optical manipulation *Nature*, **424** 810–816

[4] Molloy J E, Padgett M J 2002 Lights, action: optical tweezers *Contemp. Phys.*, **43** 241–258

[5] Dholakia K, Spalding G, MacDonald M 2002 Optical tweezers: The next generation *Phys. World* 31-35

[6] Conti C, Peccianti M, Assanto G. 2003 Route to nonlocality and observation of accessible solitons *Phys. Rev. Lett.* **91** 073901

[7] Duree G C, Shultz J L, Salamo G J, Segev M, Yariv A, Crosignani B, Di Porto P, Sharp E J, Neurgaonkar R R 1993 Observation of self-trapping of an optical beam due to the photorefractive effect *Phys. Rev. Lett.* **71** 533-536

[8] Pasquazi A, Stivala S, Assanto G, Gonzalo J, and Solis J 2008 Transverse nonlinear optics in heavy metal oxide glasses *Phys. Rev. A* **77** 043808
[9] Barsi C, Wan W, Sun C, Fleischer J W 2007 Dispersive shock waves with nonlocal nonlinearity *Opt. Lett.* **32** 2930–2932
[10] Maeso M J, Solana, J R 1993 Instabilities in the equations of state of hard-disk and hard-sphere fluids from the virial expansions *J. Chem. Phys.*, **99** 548–552
[11] Tian J, Jiang H, Gui Y, Mulero A 2009 Equation of state for hard-sphere fluids offering accurate virial coefficients *Phys. Chem. Chem. Phys.*, **11** 11213–11218
[12] Santos S, deHaro, M L, Yuste, S B 1995 An accurate and simple equation of state for hard disks *J. Chem. Phys* **103** 4622-4625
[13] Matuszewski M, Krolikowski W, Kivshar Y S 2009 Soliton interactions and transformations in colloidal media *Phys. Rev. A* **79** 023814
[14] Matuszewski M 2010 Engineering optical soliton bistability in colloidal media *Phy. Rev. A* **81** 013820
[15] Marchant T R, Smyth N F 2012 Solitary waves and their stability in colloidal media: semi-analytical solutions *Dyn. Cont. Disc. Imp. Sys.* **19** 525–541
[16] Harvey A H, Lemmon E W 2004 Correlation for the second virial coefficient of water *J. Phys. Chem. Ref. Data*, **33** 369–376
[17] Striolo A, Ward J, Prausnitz J M, Parak W J, Zanchet D, Gerion D, Milliron D, Alivisatos A P 2002 Molecular weight, osmotic Second virial coefficient, and extinction coefficient of colloidal CdSe nanocrystals *J. Phys. Chem. B*, **106** 5500–5505
[18] Striolo A, McCabe C, Cummings P T 2005 Effective interactions between polyhedral oligomeric sislesquioxanes dissolved in normal xexadecane from molecular simulation *Macromolecules* **38** 8950–8959
[19] Tian J, Gui Y 2007 Equations of state for fluids: empirical temperature dependence of the second virial coefficient *J. Phys. Chem. B* **111** 10970–10974
[20] El-Ganainy R, Christodoulides D N, Rotschild C, Segev M 2007 Soliton dynamics and self-induced transparency in nonlinear suspensions *Opt. Express* **15** 10207–10218
[21] Alberucci A, Assanto G, Buccoliero D, Desyatnikov A, Marchant T R, Smyth N F 2009 Modulation analysis of boundary induced motion of nematicons *Phys. Rev. A* **79** 043186
[22] Kath W L, Smyth N F 1995 Soliton evolution and radiation loss for the Nonlinear Schrödinger equation *Phys. Rev. E* **51** 1484–1492
[23] Minzoni A A, Smyth N F, Worthy A L 2007 Modulation solutions for nematicon propagation in non-local liquid crystals *J. Opt. Soc. Am. B* **24** 1549–1556
[24] Assanto G, Marchant T R, Smyth N F 2008 Collisionless shock resolution in nematic liquid crystals *Phys. Rev. A* **78** 063808
[25] Assanto G, Skuse B D, Smyth N F 2009 Optical path control of spatial solitary waves in dye-doped nematic liquid crystals *Photon. Lett. Poland* **1** 154–156
[26] Assanto G, Skuse B D, Smyth N F 2010 Solitary wave propagation and steering through light-induced refractive potentials *Phys. Rev. A* **81** 063811
[27] Whitham G B 1974 Linear and nonlinear waves *J. Wiley and Sons, New York*
[28] Kaplan A E 1987 Robust bistable solitons of the highly Nonlinear Shrödinger equation. *Phys. Rev. A.* **35** 455–469
[29] Carnahan N F, Starling K E 1969 Equation of State for nonattracting rigid spheres *J. Chem. Phys.* **51** 635-636
[30] Reiss H, Frisch H L, Lebowitz J L 1959 Statistical mechanics of rigid spheres *J. Chem. Phys.* **31** 369
[31] Yang J, Lakoba T I, Accelerated imaginary-time evolution methods for the computation of solitary waves *Stud. Appl. Math.,* **120** 265-292
[32] Weinstein M I 1983 Nonlinear Schrödinger equations and sharp interpolation estimates *Comm. Math. Phys.* **87** 567-576